

First-Principles Phase-Field Modeling

Jaehyeok Jin^{1,*} and David R. Reichman^{1,†}

¹*Department of Chemistry, Columbia University, New York, New York 10027, United States*

(Dated: October 11, 2024)

Phase-field methods offer a versatile computational framework for simulating large-scale microstructure evolution. However, the applicability and predictability of phase-field models are inherently limited by their *ad hoc* nature, and there is currently no bottom-up theory available that enables truly first-principles predictive modeling of large-scale non-equilibrium processes. Here, we present a bottom-up framework that provides a route to the construction of mesoscopic phase-field models entirely based on atomistic information. By introducing a molecular coarse-grained system as an intermediate step, we demonstrate the approach on the example of ice nucleation dynamics, with a spatiotemporal scale-up of nearly 10^8 times compared to the microscopic model. Our framework offers a unique approach for incorporating atomistic details into mesoscopic models, systematically bridging the gap between microscopic particle-based simulations and field-theoretic models.

Introduction—Solidification and nucleation processes involving structural and dynamical transformations that couple atomistic-level microstructure with macroscopic properties, are of pivotal importance in materials science and nanotechnology [1, 2]. However, explicating the mechanisms underlying these mesoscale processes, such as dendrite formation [3, 4] and heterogeneous nucleation [5], remains a frontier challenge. Molecular simulation offers an efficient means to elucidate microscopic factors that govern the small length scale processes underlying non-equilibrium growth processes [6]. However, brute-force particle-based simulations face clear spatiotemporal limitations beyond the molecular level.

To efficiently describe mesoscopic phase transformations, phase-field models are often used [7–10]. These models employ free energy functionals in the spirit of the Ginzburg-Landau approach [11], using simplified assumptions that lack a clear connection to the underlying microscopic physics. Given that complex structures at large length scales are ultimately connected to the underlying microscopic interactions between atoms and molecules, such approaches may encounter challenges in accurately characterizing and predicting material growth processes across various spatiotemporal scales. This issue is crucial not only for understanding solidification through the symmetry and interactions of constituent molecules [12], but also for designing novel materials, where microscopic interactions determine macroscopic properties [13]. To derive a microscopic representation, one would need to scale from the atomistic to mesoscopic levels directly [14], but this requires condensing millions of degrees of freedom into a few parameters, for which no systematic approach currently exists.

To address this challenge, we develop a bottom-up coarse-grained (CG) framework that enables the full parametrization of phase-field models from microscopic

information by introducing an intermediate molecular system. We thus begin by performing molecular coarse-graining to preserve important microscopic properties at the molecular level. Then, we apply mesoscopic coarse-graining in a hierarchical manner to attain the phase-field level representation.

Conventional Phase-Field Model—In modeling solidification, for example, the free energy functional of the phase-field model $\mathcal{F} = \int_V f(\phi)dV$ is typically expressed in terms of a single phase-field ϕ that takes values from 0 to 1 to describe two-phase systems [15–17]

$$\mathcal{F} = \int_V dV(f_{chem} + f_{doub} + f_{grad}), \quad (1)$$

where the chemical free energy density (f_{chem}) interpolates between solid (f_s) and liquid (f_l) free energies using an *ad hoc* interpolating polynomial $\bar{p}(\phi)$: $f_{chem} = \bar{p}(\phi)f_s + (1 - \bar{p}(\phi))f_l$. Conventionally, $\bar{p}(\phi) = \phi^3(10 - 15\phi + 6\phi^2)$ is adopted regardless of the system [7], as this form phenomenologically distinguishes the two phases, $\bar{p}(0) = 0$ and $\bar{p}(1) = 1$, that are locally stable $\bar{p}'(0) = \bar{p}'(1) = 0$. The double-well potential imposes the free energy barrier W at the interface as $f_{doub} = W\bar{q}(\phi)$ with another interpolating polynomial $\bar{q}(\phi) = \phi^2(1 - \phi)^2$. Lastly, the gradient free energy density f_{grad} penalizes a sharp interface with a gradient coefficient ϵ : $f_{grad} = \epsilon^2/2|\nabla\phi|^2$.

The phenomenological description of Eq. (1) can distinguish liquid ($\phi = 0$) from solid ($\phi = 1$) and is suitable for modeling various types of phase-evolution dynamics [15–17]. However, the fidelity and power of *ad hoc* approximations are questionable because the free energy quantities in Eq. (1) are typically chosen from experimental databases and not predictive [18] with the same *ad hoc* polynomials (\bar{p}, \bar{q}) used for distinct systems without considering the system dependence [19]. This limitation serves as the main motivation for this work.

Microscopic System—Water nucleation is an ideal system for our approach, due to both its significance in fields such as atmospheric chemistry [20] as well as the fact that the process is difficult to describe on long length and

* jj3296@columbia.edu

† drr2103@columbia.edu

time scales by molecular dynamics simulations [21, 22]. Thus, to demonstrate the feasibility of the proposed approach, our initial focus is on capturing crystal growth at the water-ice interface. This interface condition allows for determining the distinct free energies of each phase [Eq. (1)] concurrently, in addition to enabling the parametrization of microscopic order parameters (OPs). Here, we consider undercooled conditions to facilitate crystal growth [23].

Microscopic Order Parameter—In constructing a bottom-up phase-field model for crystal growth, it is essential to identify microscopic OPs capable of distinguishing between solid and liquid at a molecular level. At the field level, the mesoscopic OP ϕ is typically defined as a phenomenological *non-conserved* field variable, which in the case under consideration takes the value of 0 for water and 1 for ice. Due to the non-conserved nature of ϕ , its phase dynamics should follow Allen–Cahn dynamics [24], which corresponds to Model A dynamics in the classification of Hohenberg and Halperin [25]

$$\frac{\partial \phi}{\partial t} = -M_\phi \frac{\delta \mathcal{F}}{\delta \phi}, \quad (2)$$

where \mathcal{F} is the phenomenological free energy functional defined in Eq. (1), and M_ϕ determines the mobility of ϕ . Hence, to construct a microscopic phase-field model for eventual use with Eq. (2), one must first design ϕ at the molecular level. Yet, the physical definition of ϕ is unclear, making the first-principles approach challenging.

Inspired by Gaussian OPs for characterizing ice and supercooled water, we construct a “microscopic” non-conserved OP $\{\phi_I\}_I$ to distinguish the local structures of water and ice, where the local density of ice is lower compared to water [Fig. 1(c)]. We assess the fidelity of this OP for the microscopic crystal growth using trajectories efficiently sampled from bottom-up CG simulations [26–28], where single-site CG water models interact via Stillinger–Weber interactions [29] parameterized from atomistic simulations, see Supplemental Material (SM) [30]. We find that counting the local number density, ρ_I , over pair distances R_{IJ} effectively differentiates between ice and water along the CG trajectories (Fig. S3):

$$\rho_I(t) = \sum_{J \neq I} \left[\exp \left(-\frac{(R_{IJ}(t) - R_{IJ}(t))^2}{800} \right) \right], \quad (3)$$

and ϕ_I is defined on the same footing as the analytical OP form derived for crystal-melt phase coexistence [31, 32]

$$\phi_I(t) = \frac{1}{2} \left(1 - \tanh \left(\frac{\rho_I(t) - 1132}{2} \right) \right). \quad (4)$$

The constants in Eqs. (3) and (4) are *derived* from the microscopic distributions of pair distances, and they remain robust over a wide range (see Figs. S2 and S3). Figure 1(a) demonstrates that the average $\langle \rho_I(t) \rangle$ decreases

over time, and the corresponding $\{\phi_I\}_I$ can be treated as a microscopic non-conserved OP for ice growth, changing from 0.5 (indicative of ice-water mixture) to 1 over 6×10^5 CG MD timesteps (τ_{CG}). As shown later, the ability to derive free energy functionals for arbitrary (non-conserved) variables highlights the versatility of our approach and distinguishes it from classical density functional theory-based approaches [33].

Molecular Coarse-Graining—With a well-defined $\{\phi_I\}_I$, we proceed to derive the microscopic representation of the free energy functional at the CG configuration \mathbf{R}^N from the atomistic configuration \mathbf{r}^n . By introducing internal states to CG sites [34, 35], as discussed in SM Sec. III, we derive the molecular-level formulation of the phase-field free energy functional $\mathcal{F}^{CG}(\mathbf{R}^N)$:

$$\mathcal{F}^{CG} = \sum_I \mathcal{F}_I^{CG} \approx \sum_I \left(p(\phi_I) f_s(\phi_I) + (1 - p(\phi_I)) f_l(\phi_I) + f_w(\phi_I) q(\phi_I) + f_\epsilon(\phi_I) |\nabla_I \phi_I|^2 \right), \quad (5)$$

where $p_I(\phi_I)$ and $q_I(\phi_I)$ denote the local probability of the CG particle I being in the solid or at the interface, respectively. Similarly, f_s , f_l , f_w , and f_ϵ should be understood as the microscopic realizations of the free energy densities appearing in Eq. (1). Unlike conventional phase-field models, these free energy densities are not constant; rather they should be dependent on ϕ_I , correctly reflecting microscopic fluctuations of local thermodynamics in bulk phases and interfaces.

Directly determining these free energy quantities in Eq. (5) from atomistic simulations requires complex free energy sampling, which can further limit the practicality of the approach. Our CG method resolves this limitation, as the effective CG interactions are free energy-based quantities, i.e., potentials of mean force (PMFs) [36], allowing for direct parametrization from atomistic references. Inspired by force-matching for molecular coarse-graining [37], where the CG PMF is estimated by variationally matching the (unknown) forces on the CG particle I , $\mathbf{F}_I(\mathbf{R}^N)$, to the atomistic force information, $\mathbf{f}_I(\mathbf{r}^n)$, we leverage force-matching to determine the phase-field free energy functional \mathcal{F}^{CG} by minimizing the force residual:

$$\chi^2 = \frac{1}{3N} \left\langle \sum_I |\mathbf{f}_I(\mathbf{r}^n) - \mathbf{F}_I(\mathbf{R}^N)|^2 \right\rangle. \quad (6)$$

Here, $\mathbf{F}_I(\mathbf{R}^N) = -\partial \mathcal{F}^{CG} / \partial \mathbf{R}_I = -\sum_J \partial \mathcal{F}_J^{CG}(\phi_J) / \partial \mathbf{R}_I$ from Eq. (5) is further expressed using spline basis sets $\{B_k\}_k$ and coefficients $\{c_k\}_k$ [38]. With splines, any interaction $U(\phi_J)$ can be expressed as $\sum_k c_k B_k(\phi_J)$, and the effective force is obtained as $\mathbf{F}_I = -\partial U(\phi_J) / \partial \mathbf{R}_I = -(\partial U(\phi_J) / \partial \phi_J) \cdot (\partial \phi_J / \partial \mathbf{R}_I)$, where $-\partial U(\phi_J) / \partial \phi_J := -\dot{U}(\phi_J)$ can still be represented using a spline basis as $-\sum_k c_k B'_k(\phi_J)$. The objective of Eq. (6) is

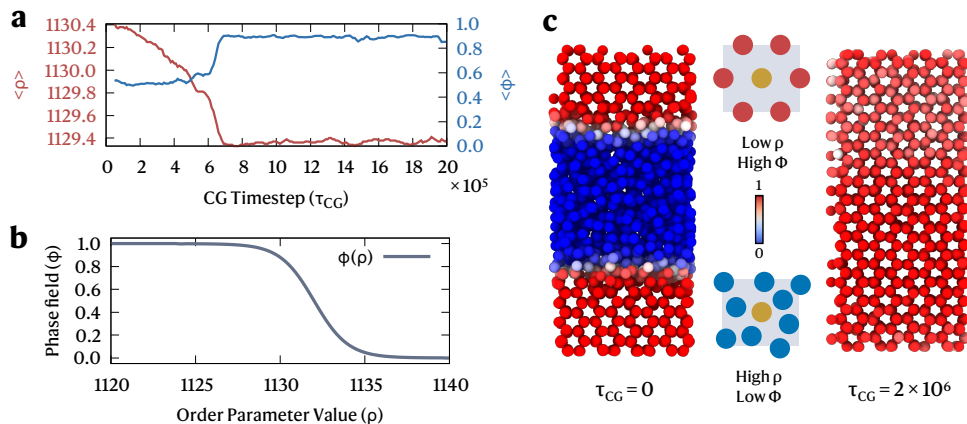


FIG. 1. Microscopic OP for ice growth at the ice-water interface ($31.50 \text{ \AA} \times 29.84 \text{ \AA} \times 68.58 \text{ \AA}$). (a) Non-conserved OP ρ using the local number density [Eq. (3)]. (b) Final profile of microscopic phase-field ϕ defined by Eq. (4). (c) $\langle \phi \rangle$ distribution of the initial configuration ($\tau_{CG} = 0$) and the final configuration ($\tau_{CG} = 2 \times 10^6$) after molecular CG simulation.

to determine the $\{c_k\}_k$ coefficients for the four force components according to Eq. (5): $\mathbf{F}_I = \mathbf{F}_I^s + \mathbf{F}_I^l + \mathbf{F}_I^w + \mathbf{F}_I^\epsilon$. For example, \mathbf{F}_I^s can be written as $-\sum_J (f_s(\phi_J)\dot{p}(\phi_J) + p(\phi_J)\dot{f}_s(\phi_J)) \partial\phi_J/\partial\mathbf{R}_I$. However, here we note that $f_s(\phi_J)$ and $p(\phi_J)$ are non-linearly coupled, and hence minimizing \mathbf{F}_I^s becomes difficult. In turn, due to the complexity of \mathbf{F}_I , especially given the nature of how the quantities $p(\phi)$ and $q(\phi)$ are connected to free energy variables, the variational determination of all terms in Eq. (6) simultaneously becomes impractical.

To surmount this difficulty, our molecular CG method employs a two-step parametrization. First, at the molecular level, we assume $p(\phi)$ and $q(\phi)$ do not deviate too far from the phenomenological description [$\bar{p}(\phi_I)$ and $\bar{q}(\phi_I)$]. This assumption allows the effective forces to be linear in terms of the unknown free energy densities $f(\phi)$, and the free energy functionals can be variationally determined. For example, $f_s(\phi_I) = \sum_k c_k^s B_k^s(\phi_I)$ can be determined via variationally optimizing $\{c_k^s\}_k$ from its force \mathbf{F}_I^s

$$\mathbf{F}_I^s = - \sum_{J,k} \left(c_k^s \left[\bar{p}(\phi_J) \frac{\partial\phi_J}{\partial\mathbf{R}_I} B_k^{s'}(\phi_J) + \dot{\bar{p}}(\phi_J) \frac{\partial\phi_J}{\partial\mathbf{R}_I} B_k^s(\phi_J) \right] \right), \quad (7)$$

which is linear in terms of c_k^s (see SM for the other cases).

Mesoscopic Coarse-Graining—Having determined the microscopic free energy densities, we now coarse-grain these quantities at the *mesoscopic* level over ϕ_I by renormalizing the values in the CG ensembles to obtain the mesoscopic-level free energy densities: $\bar{f}_s = \langle f_s(\phi_I) \rangle = -0.909$, $\bar{f}_l = -0.195$, $\bar{f}_w = 9.544$, and $\bar{f}_\epsilon = 1.004$ (all in kcal/mol). We emphasize that our CG approach correctly captures the underlying physics of solidification by satisfying $\bar{f}_s - \bar{f}_l < 0$, $\bar{f}_w > 0$, and $\bar{f}_\epsilon > 0$.

Next, with the renormalized \bar{f} , the second step of parametrization aims to determine the interpolating polynomials, $p(\phi)$ and $q(\phi)$, from the mesoscopic-

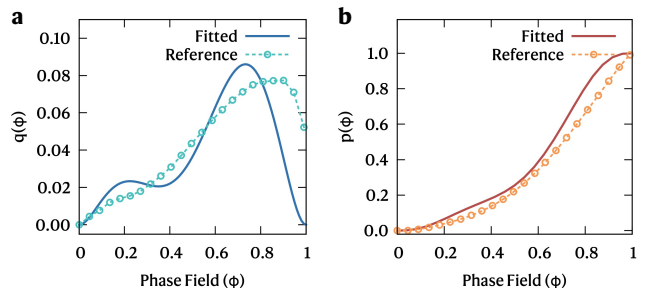


FIG. 2. Microscopically-derived interpolating polynomials: (a) $q(\phi)$ for double-well free energy and (b) $p(\phi)$ for chemical free energy. From the microscopic results (dots) numerically stable profiles were fitted using polynomials (solid lines).

level phase-field free energy functional $\mathcal{F}_{\text{meso}} := \sum_I (p(\phi_I)\bar{f}_s + (1-p(\phi_I))\bar{f}_l + \bar{f}_w q(\phi_I) + \bar{f}_\epsilon |\nabla_I \phi_I|^2)$. Akin to Eq. (7), we again perform force-matching at the mesoscopic level under constant values of \bar{f}_s , \bar{f}_l , \bar{f}_w , and \bar{f}_ϵ . As $p(\phi)$ and $q(\phi)$ are not related, and their exact microscopic forms are unknown, we sequentially determine $q(\phi)$ and then $p(\phi)$ from the initial conditions $\bar{q}(\phi)$ and $\bar{p}(\phi)$ using Eq. (6) (see SM). This sequential approach allows for incorporating system-dependent corrections for incorporating system-dependent corrections to $\bar{p}(\phi)$ and $\bar{q}(\phi)$ with a thermodynamically consistent representation [39], see Fig. 2.

Interestingly, the optimized $p(\phi)$, which interpolates between water and ice, exhibits a profile similar to the *ad hoc* $\bar{p}(\phi)$, satisfying $p(0) = 0$ and $p(1) = 1$. However, we observe notable differences between $q(\phi)$ and $\bar{q}(\phi)$. While $q(\phi)$ displays a double-well profile similar to $\bar{q}(\phi)$, it is asymmetric near $\phi = 1/2$ —as no symmetric double-well constraint is imposed—and has a metastable region near $\phi \approx 0.3$, corresponding to the plateau in the microscopic distribution (Fig. S3). In turn, Fig. 2 suggests that $q(\phi)$ generally differs from $\bar{q}(\phi)$ due to these molecular-

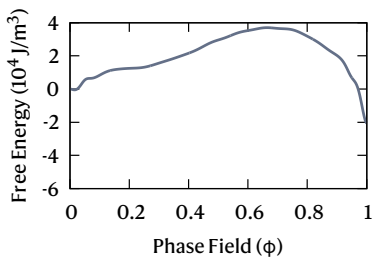


FIG. 3. Mesoscopic bulk free energy pathway underlying the ice growth at the mesoscale $p_f(\phi)\mathbb{f}_s + (1 - p_f(\phi))\mathbb{f}_l + q_f(\phi)\mathbb{f}_w$ with respect to the phase-field (ϕ).

level details. More importantly, the optimized $q(\phi)$ exhibits $q(1) \neq 0$, implying that the phase-field description can only be derived from microscopic statistics under the *additional strong assumption*: $q(1) = q'(1) = 0$. To note, non-zero $q(1)$ and $q'(1)$ values would render $q(\phi)$ locally unstable at $\phi = 1$, forcing the field simulation to propagate ϕ outside of $[0, 1]$, which is unphysical. Therefore, numerically stable polynomials for phase-field simulations are derived by fitting the obtained $p(\phi)$ and $q(\phi)$ values to polynomials $p_{PF}(\phi) = \phi^3(58.01\phi^4 - 187.37\phi^3 + 220.04\phi^2 - 113.01\phi + 23.33)$ and $q_{PF}(\phi) = \phi^2(\phi - 1)^2(15.34\phi^2 - 11.79\phi + 2.64)$, while enforcing $q_{PF}(1) = q'_{PF}(1) = 0$. Despite the deviations in Fig. 2, we will show that the fitted polynomials impart an accurate description of the growth process.

Bottom-Up Phase-Field Model—We extend the mesoscopic CG free energy functional to phase-field thermodynamics to gauge the model’s ability to reproduce nucleation. The CG bulk free energy densities (\bar{f}_s , \bar{f}_l , and \bar{f}_w in kcal/mol) can be directly scaled up to mesoscopic energy densities (f in J/m³) by averaging CG energetics over the molecular volume. Due to its thermodynamic consistency (by design), our method can predict whether the system will exhibit one phase ($f_l < f_s$) or two phases ($f_l > f_s$) at different temperatures. In Fig. 3, a positive energy barrier, $\mathbb{f}_w = 1.030 \times 10^6$ J/m³, and a stable solid phase, $\mathbb{f}_l - \mathbb{f}_s = 7.699 \times 10^4$ J/m³, are indicative of nucleation, with the broad transition state profile consistent with the free energy pathway for the phase-field model of an undercooled Ni melt [17].

Unlike bulk quantities, directly mapping the interface energy density \bar{f}_ϵ to the mesoscopic interface term, $\mathbb{f}_\epsilon := \bar{e}^2/2$, is not feasible due to the significant scale difference between the molecular-level thickness ($< \text{nm}$) and the mesoscopic interface width δ ($\sim \mu\text{m}$). Nevertheless, by assuming steady-state interface growth, the gradient energy coefficient \bar{e} can be determined from mesoscopic physical properties [40, 41]. In doing so, we first build a phase-field level mesoscopic interface ($30 \mu\text{m} \times 65 \mu\text{m}$) from the atomistic level ($2.98 \text{ nm} \times 6.86 \text{ nm}$) with a similar aspect ratio, achieving nearly a 10^8 scale-up [Fig. 4(a)]. To note, even with coarse-graining, particle-based

CG models would be challenged to reach such spatiotemporal scales.

To discretize the phase-field system onto numerical grids, we chose a lattice size of $\Delta x = 0.5 \mu\text{m}$ following typical values for pure materials [42] to realize an interface thickness of $\delta = 4\Delta x$, covering $\lambda = 0.1 < \phi < 1 - \lambda$. Under the steady-state approximation [41], \bar{e} is related to δ via the interface region parameter $b = 2\tanh^{-1}(1 - 2\lambda)$ such that $\bar{e} = \sqrt{3\delta\gamma/b}$, where the interface energy γ between phases is linked to \mathbb{f}_w with $\gamma = (\mathbb{f}_w\delta)/(6b)$ (see SM Sec. V). Taken together, the mesoscopic interface term is estimated as $\bar{e} = 6.5306 \times 10^{-4} \text{ J}^{1/2}/\text{m}^{1/2}$. Having determined \mathbb{f}_w and \mathbb{f}_ϵ , the initial condition $\phi_0(r\Delta x)$ from the center of the interface follows the equilibrium profile by solving $\partial\phi/\partial t = 0$

$$\phi_0(r\Delta x) = \frac{1}{2} \left[1 - \tanh \left(\sqrt{\frac{\mathbb{f}_w}{\mathbb{f}_\epsilon}} r\Delta x \right) \right] = \frac{1 - \tanh(0.549r)}{2}, \quad (8)$$

with a thickness of about $4 \mu\text{m}$ as depicted in Fig. 4(b).

Our approach provides a well-defined and useful segue from the description of the molecular system to the field-level simulation of Model A dynamics. Equation (2) was propagated using the microscopically-derived free energy functional $\mathcal{F}_{PF} = \int_V dV (p_{PF}(\phi)\mathbb{f}_s + (1 - p_{PF}(\phi))\mathbb{f}_l + \mathbb{f}_w q_{PF}(\phi) + \mathbb{f}_\epsilon |\nabla\phi|^2)$ and the phase-field mobility $M_\phi = 0.366 \text{ m}^3 \cdot \text{J}^{-1} \text{ s}^{-1}$ based on conventional settings with an interfacial mobility of $10^{-6} \text{ m}^4 \cdot \text{J}^{-1} \text{ s}^{-1}$ (see SM Sec. V) that determines the effective timestep τ_{PF} [43]. Remarkably, Fig. 4(c) shows that our *ab initio* phase-field model recapitulates the fully crystallized ice phase ($\tau_{PF} = 2000$), evolving from the ice-water interface ($\tau_{PF} = 0$), consistent with molecular-level phenomena. This finding underscores that the proposed approach can accurately predict crystal growth at the mesoscale based entirely on detailed microscopic interactions, without relying on experimental observations.

Conclusion—We have presented a novel first-principles framework for deriving mesoscopic phase-field models entirely grounded in microscopic dynamics [44]. This microscopic-mesosopic link, spanning eight orders of spatiotemporal scales, is established by introducing a molecular CG description in a hierarchical manner. Our framework requires only microscopic simulations without the need for *ad hoc* thermodynamic parameters. While our findings suggest that deriving conventional phase-field models from full microscopic physics may necessitate several approximations in free energy functionals, they also offer new insights into developing *ab initio* phase-field models for more complex microscopic dynamics. Since our methodology is readily generalizable to any arbitrary phase dynamics, e.g., multi-phase-field [45] or phase-field crystal models [46], we anticipate this work will extend beyond the scope of rigorous coarse-graining with applications to new classes of mesoscopic materials

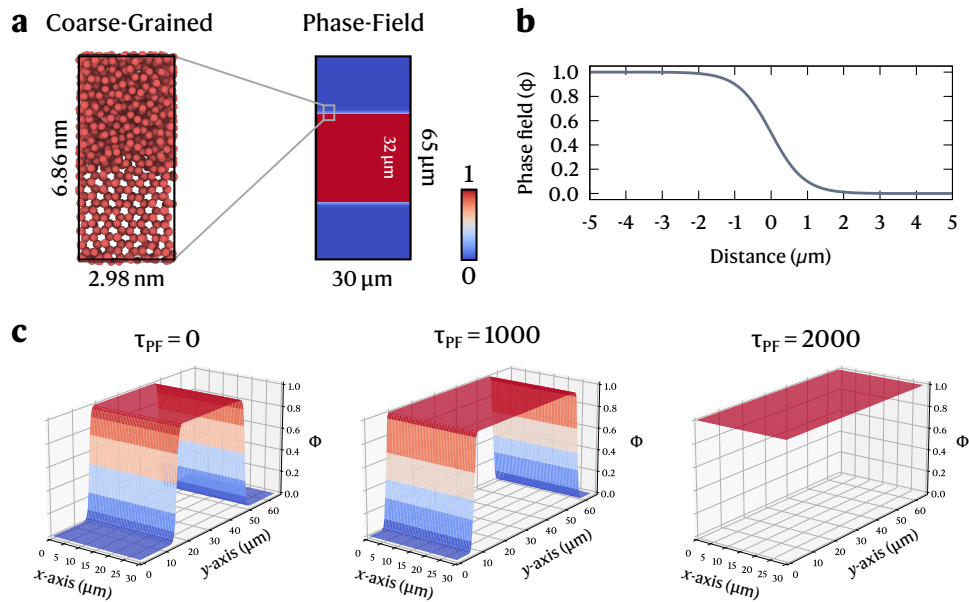


FIG. 4. Microscopically-derived phase-field model for ice growth. (a) Scaling up the molecular CG interface to the phase-field level. (b) Equilibrium profile of phase-field ϕ from the center of interface. (c) Time evolution of ϕ driven by microscopically-derived free energy functional using Model A dynamics [Eq. (2)], where τ_{PF} is the phase-field timestep ($\phi = 1$: ice, 0: water).

and phenomena.

J.J. thanks the Arnold O. Beckman Postdoctoral Fellowship for funding and academic support.

-
- [1] J. W. Martin, R. D. Doherty, and B. Cantor, *Stability of microstructure in metallic systems* (Cambridge University Press, 1997).
- [2] B. L. Altshuler, P. A. Lee, and W. R. Webb, *Mesoscopic phenomena in solids* (Elsevier, 2012).
- [3] J. S. Langer, *Rev. Mod. Phys.* **52**, 1 (1980).
- [4] S. David and T. DebRoy, *Science* **257**, 497 (1992).
- [5] K. Kelton and A. L. Greer, *Nucleation in condensed matter: applications in materials and biology* (Elsevier, 2010).
- [6] M. F. Horstemeyer, Multiscale modeling: A review, in *Practical Aspects of Computational Chemistry: Methods, Concepts and Applications*, edited by J. Leszczynski and M. K. Shukla (Springer Netherlands, Dordrecht, 2010) pp. 87–135.
- [7] J. Langer, in *Directions in condensed matter physics: Memorial volume in honor of shang-keng ma* (World Scientific, 1986) pp. 165–186.
- [8] L.-Q. Chen, *Annu. Rev. Mater. Res.* **32**, 113 (2002).
- [9] N. Moelans, B. Blanpain, and P. Wollants, *CALPHAD* **32**, 268 (2008).
- [10] I. Steinbach, *Annu. Rev. Mater. Res.* **43**, 89 (2013).
- [11] V. L. Ginzburg and L. Landau, *Zh. Eksp. Teor. Fiz.* **20**, 1064 (1950).
- [12] D. R. Nelson, *Defects and geometry in condensed matter physics* (Cambridge University Press, 2002).
- [13] R. Wittkowski, H. Löwen, and H. R. Brand, *Phys. Rev. E* **84**, 041708 (2011).
- [14] We note that, in principle, an even more microscopic approach could be based on density functional theory [47]. However, this framework is quite distant from describing all types of growth dynamical behavior, including non-conserved order parameters, which is the primary focus of this work.
- [15] W. J. Boettinger, J. A. Warren, C. Beckermann, and A. Karma, *Annu. Rev. Mater. Res.* **32**, 163 (2002).
- [16] T. Takaki, *ISIJ Int.* **54**, 437 (2014).
- [17] L. Gránásy, G. I. Tóth, J. A. Warren, F. Podmaniczky, G. Tegze, L. Rátkai, and T. Pusztai, *Prog. Mater. Sci.* **106**, 100569 (2019).
- [18] N. Saunders and A. P. Miodownik, *CALPHAD (calculation of phase diagrams): a comprehensive guide* (Elsevier, 1998).
- [19] M. Plapp, *Phil. Mag.* **91**, 25 (2011).
- [20] D. Rosenfeld, *Science* **287**, 1793 (2000).
- [21] K. Kelton (Academic Press, 1991) pp. 75–177.
- [22] M. Matsumoto, S. Saito, and I. Ohmine, *Nature (London)* **416**, 409 (2002).
- [23] C. A. Angell, Supercooled water, in *Water and Aqueous Solutions at Subzero Temperatures*, edited by F. Franks (Springer US, Boston, MA, 1982) pp. 1–81.
- [24] S. M. Allen and J. W. Cahn, *Acta Metall.* **27**, 1085 (1979).
- [25] P. C. Hohenberg and B. I. Halperin, *Rev. Mod. Phys.* **49**, 435 (1977).
- [26] H. Wang, C. Junghans, and K. Kremer, *Eur. Phys. J. E* **28**, 221 (2009).
- [27] J. Jin, Y. Han, A. J. Pak, and G. A. Voth, *J. Chem. Phys.* **154**, 044104 (2021).
- [28] J. Jin, A. J. Pak, Y. Han, and G. A. Voth, *J. Chem. Phys.* **154**, 044105 (2021).
- [29] F. H. Stillinger and T. A. Weber, *Phys. Rev. B* **31**, 5262 (1985).
- [30] See Supplemental Material for details on the microscopic

- derivation of the CG Hamiltonian (Sec. II) and the simulation details for atomistic system (Sec. III), as well as parametrization details for molecular and mesoscopic coarse-graining (Sec. IV) and phase-field simulation (Sec. V).
- [31] W. Shih, Z. Wang, X. Zeng, and D. Stroud, *Phys. Rev. A* **35**, 2611 (1987).
- [32] M. Iwamatsu and K. Horii, *J. Phys. Soc. Jpn.* **65**, 2311 (1996).
- [33] T. Ramakrishnan and M. Yussouff, *Phys. Rev. B* **19**, 2775 (1979).
- [34] J. F. Dama, J. Jin, and G. A. Voth, *J. Chem. Theory Comput.* **13**, 1010 (2017).
- [35] J. Jin and G. A. Voth, *J. Chem. Theory Comput.* **14**, 2180 (2018).
- [36] J. Jin, A. J. Pak, A. E. Durumeric, T. D. Loose, and G. A. Voth, *J. Chem. Theory Comput.* **18**, 5759 (2022).
- [37] W. G. Noid, J.-W. Chu, G. S. Ayton, V. Krishna, S. Izvekov, G. A. Voth, A. Das, and H. C. Andersen, *J. Chem. Phys.* **128**, 244114 (2008).
- [38] L. Lu, S. Izvekov, A. Das, H. C. Andersen, and G. A. Voth, *J. Chem. Theory Comput.* **6**, 954 (2010).
- [39] S.-L. Wang, R. F. Sekerka, A. A. Wheeler, B. T. Murray, S. R. Coriell, R. J. Braun, and G. B. McFadden, *Physica D* **69**, 189 (1993).
- [40] J. A. Warren and W. J. Boettinger, *Acta Metall. Mater.* **43**, 689 (1995).
- [41] T. Takaki, T. Fukuoka, and Y. Tomita, *J. Cryst. Growth* **283**, 263 (2005).
- [42] A. A. Wheeler, B. T. Murray, and R. J. Schaefer, *Physica D* **66**, 243 (1993).
- [43] The reader may note that we do not address the parametrization of M_ϕ from first principles in this work. However, the relative time can be understood by rescaling the timescale τ_{PF} . A rigorous determination of M_ϕ is currently being pursued by the authors using a microscopic time-dependent projection operator approach.
- [44] The source code can be found in <https://github.com/jaehyeokjin/Bottom-up-Phase-Field>.
- [45] I. Steinbach, F. Pezzolla, B. Nestler, M. Seeßelberg, R. Prieler, G. J. Schmitz, and J. L. Rezende, *Physica D* **94**, 135 (1996).
- [46] K. R. Elder, N. Provatas, J. Berry, P. Stefanovic, and M. Grant, *Phys. Rev. B* **75**, 064107 (2007).
- [47] M. te Vrugt, H. Löwen, and R. Wittkowski, *Adv. Phys.* **69**, 121 (2020).